Physics of Plasmas

RESEARCH ARTICLE | AUGUST 30 2023

# Intermittency at Earth's bow shock: Measures of turbulence in quasi-parallel and quasi-perpendicular shocks

J. Plank ; I. L. Gingell



*Phys. Plasmas* 30, 082906 (2023)
https://doi.org/10.1063/5.0160439

# Intermittency at Earth's bow shock: Measures of turbulence in quasi-parallel and quasi-perpendicular shocks

Cite as: Phys. Plasmas **30**, 082906 (2023); doi: 10.1063/5.0160439
Submitted: 1 June 2023 · Accepted: 5 August 2023 ·
Published Online: 30 August 2023

View Online Export Citation CrossMark

J. Plank[a] and I. L. Gingell

## AFFILIATIONS

Department of Physics and Astronomy, University of Southampton, Southampton SO17 1BJ, United Kingdom

[a]Author to whom correspondence should be addressed: j.plank@soton.ac.uk

## ABSTRACT

Turbulent plasmas such as the solar wind and magnetosheath exhibit an energy cascade that is present across a broad range of scales, from the stirring scale at which energy is injected, down to the smallest scales where energy is dissipated through processes such as reconnection and wave–particle interactions. Recent observations of Earth's bow shock reveal a disordered or turbulent transition region exhibiting features of turbulent dissipation, like reconnecting current sheets. We used observations from magnetospheric multiscale (MMS) over four separate bow shock crossings of varying shock normal angle to characterize turbulence in the shock transition region and how it evolves toward the magnetosheath. These cases studies have been chosen to ensure validity of Taylor's hypothesis, which we discuss in depth. We observe the magnetic spectrum evolving by fitting power laws over many short intervals, finding that the power-law index in the shock transition region is separable from the upstream and downstream plasma, for both quasi-perpendicular and quasi-parallel shocks. Across the shock, we see a change in the breakpoint location between inertial and ion power-law slopes. We also observe the evolution of scale-independent kurtosis of magnetic fluctuations across the shock, finding a reduction of high kurtosis intervals downstream of the shock. Finally, we adapt a method for calculating correlation length to include a high-pass filter, allowing estimates for changes in correlation length across the shock. In a quasi-perpendicular shock, we find the correlation length to be significantly smaller in the magnetosheath than in solar wind; however, the opposite can occur for quasi-parallel shocks.





## I. INTRODUCTION

Turbulence is a ubiquitous phenomenon in space plasmas, occurring in systems ranging from star formation[1] to galaxy clusters[2] to planetary magnetospheres[3] and the solar wind.[4–6] In collisionless plasmas such as the solar wind, the mechanisms for dissipating energy in turbulence are not well known,[6] and solving this problem is vital for our understanding of turbulence in general. In the heliosphere, for example, turbulent dissipation is a suggested source of the heating observed in the solar corona.[7,8] One of several proposed solutions to this dissipation problem is magnetic reconnection,[9,10] in which local changes in magnetic topology rapidly transfer energy from fields to particles, resulting in particle acceleration and heating.[11–15] Some other possible explanations for energy dissipation include wave–particle interactions, driven by cyclotron resonance or kinetic Alfvén waves.[16,17]

One advantage of using the local space environment to study plasma turbulence is that it allows for high-cadence *in situ* observation of structures associated with turbulent dissipation, such as reconnecting current sheets. The magnetospheric multiscale (MMS) mission has recently been used to observe electron outflow jets at thin current sheets—a signature of reconnection—in Earth's magnetosheath[18] and the bow shock transition region.[19,20] Recent simulations[21–24] have shown that processes in the shock foot can generate current sheets and magnetic islands, contributing to the formation of a transition region that can appear turbulent. The properties of turbulence are also known to vary across different plasma regimes, such as the solar wind and magnetosheath.[25] Furthermore, the properties of turbulence are also known to vary within the magnetosheath, varying with the upstream shock orientation[26] and between the sub-solar point and flanks.[27,28] Hence, these observations of turbulence and coherent structures in the shock layer, and differences in the characteristics of turbulence throughout the magnetosheath together raise two open questions: (1) Is there a measurable difference between turbulence seen in the bow

shock transition region and in the surrounding plasma (i.e., the solar wind and magnetosheath)? (2) How quickly does well-developed turbulence arise in the magnetosheath after a bow shock crossing? For both of these questions, we also compare the differences between quasi-parallel and quasi-perpendicular shocks.

We note that some definitions of turbulence require a "well-developed" inertial range, allowing a complete cascade from the largest, fluid-like scales in the plasma, through the kinetic regime and ending at the dissipation scale. In the shock transition region, disordered fluctuations may be driven by non-linear interactions and instabilities that arise at scales smaller than the inertial range, but nevertheless appear to cascade and dissipate energy in the region. In this study, we will refer to these processes as turbulent; however, it is possible that they will not always fit the definition of fully developed turbulence.

In this paper, we address the aforementioned observations by studying the evolution of magnetic fluctuations from the solar wind to magnetosheath, i.e., across the bow shock, using three different measures of turbulence: the magnetic spectrum, the kurtosis, and the correlation length (e.g., Ref. 29). From the magnetic spectrum, we extract the spectral break between inertial and ion scale ranges, which is related to local plasma scales such as the ion gyroradius $\rho_i$ and inertial length $d_i$.[30,31] We found that the magnetic spectrum in the shock transition region was steeper than both upstream and downstream regions at the electron scale in the quasi-perpendicular event. Observing scale-independent kurtosis, we saw consistent evidence for intermittency in the solar wind and transition region for both quasi-parallel and quasi-perpendicular shocks, with peak kurtosis in the shock foot. Finally, we use an adapted method of calculating correlation length to measure the local coherence scale of the plasma and find significant differences between upstream and downstream turbulence. Addressing the time taken to reach well-developed turbulence, Kolmogorov-like spectral power laws arise in the inertial range approximately 30 s (or $1.6R_E$, $260d_i$) downstream of the shock in the quasi-perpendicular case, while for the quasi-parallel shock the time is closer to 2 min ($6.2R_E$, $1300d_i$). However, the correlation length transitioned almost instantaneously across the shock for the quasi-perpendicular shock, but took 1–2 min for the quasi-parallel shock.

## II. DATA SET

We explore the bow shock transition using *in situ* data obtained by the magnetospheric multiscale (MMS) mission.[32] Magnetic field data are provided by the flux gate magnetometer (FGM)[33] and search coil magnetometer (SCM).[34] FGM and SCM data are analyzed as a merged data set (FSM).[35] Particle data are provided by the fast plasma investigation's (FPI)[36] dual electron spectrometer (DES) and dual ion spectrometer (DIS). In high-resolution burst mode, the SCM and FSM magnetic fields are available at a sampling cadence of $f_s = 1/8192$ s, while FGM is available at 1/128 s. Particle moments are available at a cadence of 0.15 and 0.03 s for ions and electrons, respectively.

Four high-resolution (burst) bow shock crossing intervals have been analyzed here. The events were chosen to cover a range of bow shock angles from quasi-perpendicular to quasi-parallel, where the burst interval was longer than approximately 10 min. Event D was found with the help of a database of 2797 shocks compiled using machine learning from Ref. 37. These four shocks were chosen first due to the intervals each recording sufficient burst data both upstream and downstream of the shock, allowing us to observe the evolution. Second, they all performed well on the test of Taylor's hypothesis, which is described further in Sec. II A. Figure 1 provides a summary of events A–D, ordered from most quasi-perpendicular to most quasi-parallel. The intervals on 13 March 2018, 16 March 2018, 18 March 2020, and 14 February 2020 are referred to as intervals A, B, C, and D,

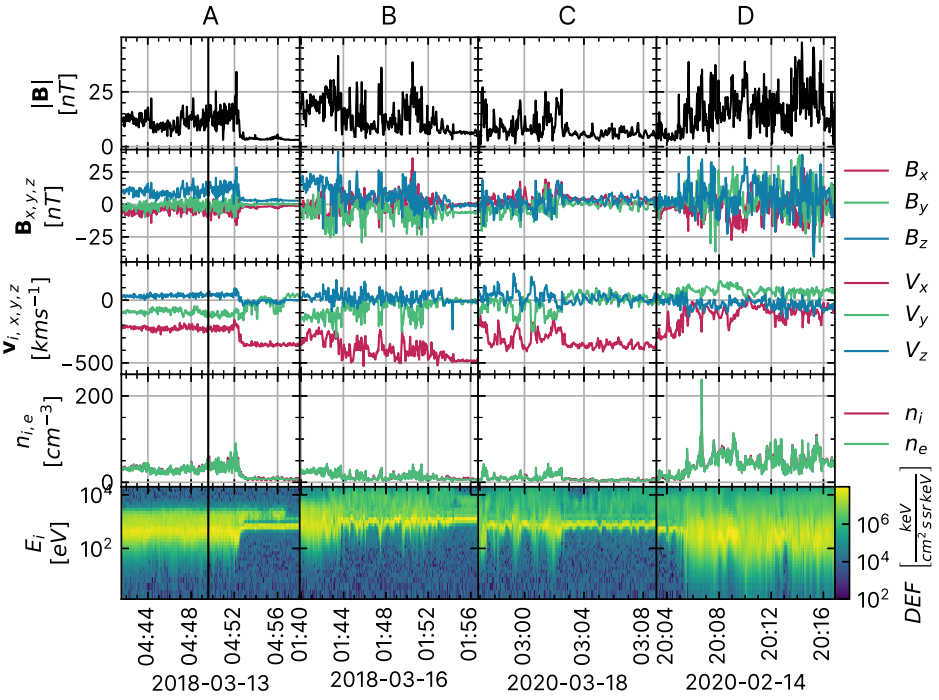


**FIG. 1.** MMS observations showing events A (left column) to D (right column). Row 1: magnetic field strength, $|\mathbf{B}|$; row 2: magnetic field components, $\boldsymbol{B}$, in GSE coordinates; row 3: ion velocity components, $v_i$ (GSE); row 4: proton and electron densities, $n_{i,e}$; row 5: ion energy spectrogram. In events A–C, MMS travels from magnetosheath to solar wind, and in event D, MMS travels from solar wind to magnetosheath. The shock normal angles are $\theta_{Bn} = 68°$, 41°, 35°, and33° for A–D, respectively. The timestamp of Fig. 3 is indicated by a vertical black line in column A.

**TABLE I.** Average upstream plasma properties as observed by OMNI and MMS. Data from OMNI were averaged over the same duration as MMS.

| Interval | $\theta_{Bn}$ (deg) | $v_0$ (km s$^{-1}$) | $M_A$ | $\beta_i$ | Start yyyy/mm/dd hh:mm:ss | End |
|---|---|---|---|---|---|---|
| A | 68 ± 0.6 | 356.4 ± 1.0 | 14.6 ± 1.1 | 4.4 ± 0.7 | 2018/03/13 04:41:33 | 04:58:02 |
| B | 41 ± 3.0 | 475.8 ± 4.7 | 9.0 ± 0.7 | 1.4 ± 0.3 | 2018/03/16 01:39:53 | 01:56:43 |
| C | 35 ± 1.1 | 394.4 ± 3.9 | 9.8 ± 0.8 | 2.2 ± 0.5 | 2020/03/18 02:56:53 | 03:08:52 |
| D | 33 ± 0.8 | 330 ± 2.4 | 14.6 ± 0.3 | 1.1 ± 0.9 | 2020/02/14 20:03:13 | 20:16:52 |

respectively. Note that electron moments are not available for MMS 4 during event D. All events are ∼15 min in duration. Table I shows plasma parameters averaged over the entire upstream interval, which includes electron upstream flow speed $v_0$, the acute angle between upstream magnetic field **B**, the shock normal $\theta_{Bn}$, Alfvén Mach number $M_A$ of the upstream flows, and the ion plasma beta $\beta_i$. The derived parameters $M_A$ and $\beta_i$, along with observed values for $v_0$ and the magnetic field, were obtained from OMNI.[38] The shock angle $\theta_{Bn}$ was calculated using a model from Ref. 39, using the upstream magnetic field lagged to the bow shock from OMNI and FPI moments from MMS. Sample standard errors on the angle were low for each of the events, with a maximum of ±3.0° for event B. Also note that the upstream solar wind is slow for all four events, in particular A and D. Consequently, the results discussed here may not be valid for the alternative case of a fast upstream flow.

The angle between the upstream magnetic field and shock normal angle, $\theta_{Bn}$, decreases from quasi-perpendicular (68°) in event A to quasi-parallel (33°) in event D. Quasi-perpendicular shocks are characterized by near discontinuous transitions from the solar wind to bow shock. In contrast, a quasi-parallel shock has a more gradual transition and can often be complicated by upstream waves and instabilities caused by backstreaming ions in the foreshock. Therefore, the expectation is that structures created by the shock are more distinct in quasi-perpendicular shock crossings but are only observed for a short time, whereas a quasi-parallel shock will display complex behavior that is more challenging to separate from the solar wind or magnetosheath.

### A. Validity of Taylor's hypothesis

The interpretation of results in Sec. III relies on the validity of transforming the temporal domain measurements from MMS1 into the spatial domain, using the Taylor hypothesis.[40] The assumption is that fluctuations will travel past the spacecraft at a bulk flow speed $v_0$ that is much greater than the wave propagation speeds; thus, the spatial configuration of the fluctuations is unchanging as they are swept past the spacecraft. For plasmas with a fast flow speed, $v_0 \gg v_A$, such as the solar wind, this assumption is well founded. However, for plasmas such as the magnetosheath and the bow shock, Taylor's hypothesis may not be valid.

The increments of the magnetic field, $\delta\boldsymbol{B}$, are given by

$$\delta\boldsymbol{B}(\tau) = \langle|\boldsymbol{B}(t+\tau) - \boldsymbol{B}(t)|\rangle_T, \tag{1}$$

where $\tau$ represents the time lag and $\langle\rangle_T$ represents the mean over the full time interval. The lag $\tau$ can be transformed into spatial lag $\ell$ according to Taylor's hypothesis using the bulk flow speed: $\ell = v_0 t$. In this case, $v_0$ is the mean bulk velocity in each region (solar wind, bow shock transition, or magnetosheath).

We can also measure the magnetic field increments for spatial lag $\ell$ directly using the separation between spacecraft pairs, without needing to assume Taylor's hypothesis.[29,41–45] The equation in this case is then

$$\delta\boldsymbol{B}(\ell_{ij}) = \langle|\boldsymbol{B}^i(t) - \boldsymbol{B}^j(t)|\rangle_T, \tag{2}$$

where $i, j = 1, 2, 3, 4$ are labels for each of the four spacecraft; thus, $ij$ indicates one of the six spacecraft pairs, and $\boldsymbol{B}^i$ indicates the magnetic field vector as measured by spacecraft $i$. We are, therefore, able to test the validity of Taylor's hypothesis by direct comparison of the amplitude of the magnetic field increments for single-spacecraft and multi-spacecraft measures. However, the nature of this test means that comparisons can only be made for scales close to the separation of the six MMS pairs. Therefore, good performance of this test at the spacecraft separation scales does not necessarily guarantee good performance at larger or smaller spatial scales.

We assess the validity of Taylor's hypothesis separately in each of the three regions (upstream, shock, and downstream) for events A and D here, in Fig. 2, with corresponding plots for events B and C shown in the supplementary material, Fig. S1. Figure 2 shows magnetic fluctuation amplitude normalized to average field strength, $|\delta\boldsymbol{B}|/B_0$, for both single spacecraft and for the six spacecraft pairs (as in Ref. 42).

We found that all events performed reasonably well at the available spacecraft separation scales, particularly in the magnetosheath. The shock transition in event A sees the fluctuation amplitude slightly underestimated. Chasapis *et al.*[41] reason that at small scales the two-spacecraft estimate cannot be suitably averaged such that the spatial statistics are homogeneous, allowing for the presence of strong gradients between spacecraft to affect the structure function. Single-spacecraft estimates can only be affected by gradients in the direction of plasma flow and hence could report a lower value, even if Taylor's hypothesis is still valid. For example, this could happen in the case of an anisotropy in $\boldsymbol{B}$. Since MMS is in a tetrahedral formation for all four events, then in general, the multi-spacecraft method will not be aligned with the direction of plasma flow and may instead be observing different fluctuations to the flow-aligned Taylor method. In the solar wind in event A, it appears the plasma encountered by MMS 1 and 2 compared to MMS 3 and 4 was slightly different, leading to two different groups of single-spacecraft lines. Event D performs best overall with single-spacecraft measurements in all regions being very close to the multi-spacecraft results. Stawarz *et al.*[45] consider a ratio of $D^{(2)}_{\text{multi}}/D^{(2)}_{\text{taylor}} \leq 2$ (where $D^{(2)} = |\delta\boldsymbol{B}|/B_0$, i.e., the second order structure function) to be the threshold for accepting the validity of Taylor's hypothesis. In fact, they consider this only for spacecraft pairs that form an angle of less than 5° of the flow direction, since for angles

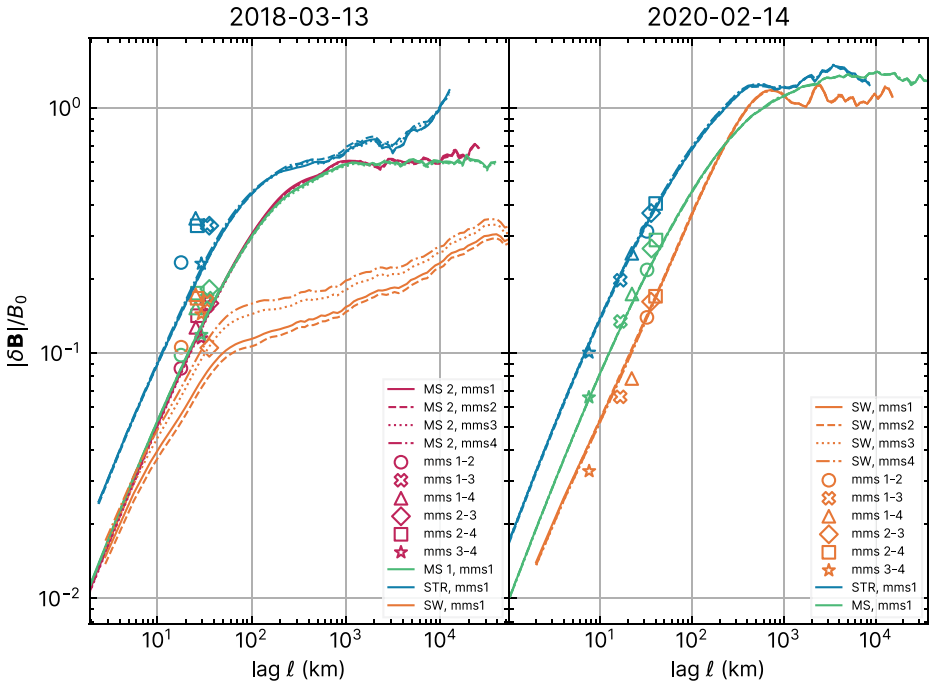


**FIG. 2.** Magnetic fluctuation amplitude normalized to average field strength, $|\delta \boldsymbol{B}|/B_0$ as a function of scale $\ell$. Left: event A, right: event D. Fluctuation amplitudes obtained using a single spacecraft and assuming Taylor's hypothesis are given by a line, solid for MMS 1, dashed for MMS 2, dotted for MMS 3, and dotted–dashed for MMS 4. Colors represent the different regions of each event: orange for solar wind (SW), blue for shock transition region (STR), and green/red for the magnetosheath (MS). Measurements from the six spacecraft pairs, with $\ell$ equivalent to the separation scale, are shown by the following markers: circle for MMS 1–2, cross for 1–3, triangle for 1–4, diamond for 2–3, square for 2–4, and star for 3–4. In event A, the single-spacecraft and multi-spacecraft results are reasonably similar, within a factor of two, particularly in the magnetosheath. The results for event D are also extremely close at all scales and for all regions.

greater than this the disparity could be even greater while the hypothesis is still valid, as discussed above. However, since the averages for all our events lie within this factor of two, we consider them to be valid without adjusting for the angle relative to $\boldsymbol{v_0}$, which would reduce the ratio even further.

### 1. Influence of whistler-mode waves at sub-ion scales

The importance of a fast flow, as discussed above, is not the only consideration when dealing with Taylor's hypothesis. The validity condition, as shown by Howes *et al.*,[46] is

$$\frac{v_0}{v_A}\cos(\theta) \gg \frac{\omega}{k v_A}, \tag{3}$$

where $v_A$ is the Alfvén speed, $\theta$ denotes the angle between a wavevector $\boldsymbol{k}$ and the bulk flow velocity $\boldsymbol{v_0}$, $\omega$ is the wave frequency, and $k$ is wavenumber. From this, we see that Taylor's hypothesis can be invalid in the slow flow regime (LHS), discussed above, as well as in the dispersive regime (RHS), when frequency increases faster than linearly with wavenumber.

It was also shown by Howes *et al.*[46] that ion cyclotron waves and kinetic Alfvén waves are not likely to violate Taylor's hypothesis, but whistler-mode waves can under some circumstances. The dispersion relation for whistler waves can be well estimated by

$$\omega = k v_A \sqrt{1 + (k_\parallel d_i)^2}. \tag{4}$$

Leading to a TH validity condition of

$$\frac{v_0}{v_A}\cos(\theta) \gg \sqrt{1 + (k_\parallel d_i)^2}. \tag{5}$$

This can be simplified given that the RHS will only be significant when $k_\parallel d_i \gg 1$. Additionally, whistler waves occur in the regime $k_\parallel \geq k_\perp$, allowing a projection of $\boldsymbol{k}$ along the $\hat{\boldsymbol{v_0}}$ direction to be used, $k_\parallel \cos(\theta) \approx k \cos(\theta) \approx k_{\text{eff}}$. This results in an observable validity condition for the Taylor hypothesis[46]

$$\frac{v_0}{v_A}\cos^2(\theta) \gg k_{\text{eff}} d_i. \tag{6}$$

Taking $\cos(\theta) \approx 1$ and using the appropriate values from event A of $v_0 = 356.4\,\text{km s}^{-1}$, $v_A = 20.7\,\text{km s}^{-1}$, and $d_i = 38.6$ km, we find that whistler waves occurring at

$$k_{\text{eff}} \gg 0.44\ \text{km}^{-1} \tag{7}$$

are likely to violate Taylor's hypothesis. Similarly, for event D, we find that when $v_0 = 330\,\text{km s}^{-1}$, $v_A = 56.2\,\text{km s}^{-1}$, and $d_i = 31.4$ km, then

$$k_{\text{eff}} \gg 0.19\,\text{km}^{-1}. \tag{8}$$

For event A, this would correspond to scales around $d_e$, while for event D this is roughly halfway between $\log(1/d_i)$ and $\log(1/d_e)$. In Fig. 3, there is an example of a wave peaking at $2\,\text{km}^{-1}$ which, if it is a whistler wave,[47] likely has some effect on the validity of Taylor's hypothesis. However, while it is important to note that Taylor's hypothesis becomes less directly applicable at scales smaller than the electron inertial length, particularly at times of strong whistler activity, we do not believe it has a significant effect on the validity or interpretation of our results, which focus primarily on ion scales at $k \approx 0.02\,\text{km}^{-1}$.

Compressible Hall-MHD simulations performed by Perri *et al.*[48] showed that a violation of Taylor's hypothesis can result in a flattening of the power spectrum at scales smaller than $d_i$. Another work by

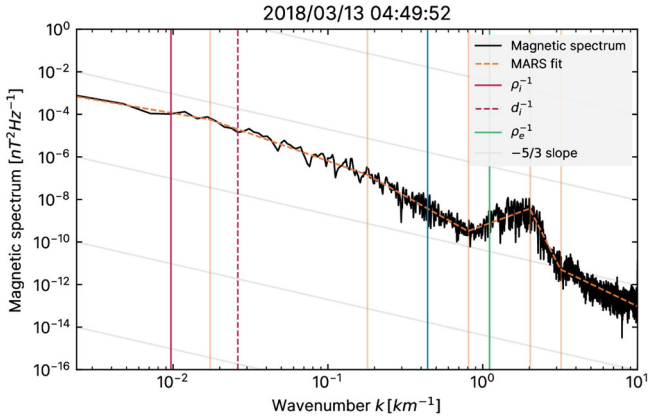


**FIG. 3.** A plot of magnetic spectrum for an example ∼6 s window downstream of the shock on 13 March 2018, illustrated as a vertical black line on Fig. 1. Grid lines are shown with a slope of −5/3. The magnetic spectrum is shown in black. The ion and electron scales ($\rho_{i,e}$ and $d_i$) are shown as red and green vertical lines. The fit to the spectrum is shown as an orange dashed line, built from chained linear regressions using the MARS method. Vertical orange lines highlight breakpoints determined by the MARS fit. An electron scale wave is visible at approximately $k \approx 2/\rho_e$, and this is reflected in the MARS fit by steep upward and downward slopes. The part of the spectrum which exceeds the noise floor at $k \approx 10\,\mathrm{km}^{-1}$ has been excluded from this plot. A blue vertical line has been drawn at $k = 0.44\,\mathrm{km}^{-1}$, indicating the scale at which whistler waves may start to violate the Taylor hypothesis.

Huang and Sahraoui[49] using a model based on observations of CLUSTER data[50] showed that a violation of Taylor's hypothesis at electron scales would shift the electron scale spectral break in the electric power spectrum to higher frequencies in the spacecraft frame. Therefore, we expect that in our data, the consequence of any violation of Taylor's hypothesis at scales smaller than the spacecraft separation scale would be a shallower power law index at around the electron inertial length and a migration of the electron scale break point toward larger $k$.

## III. THE MAGNETIC SPECTRUM

To examine the evolution of the magnetic spectrum, events A–D were split into consecutive, non-overlapping windows containing 6 s of data per window. There are 145, 112, 79, and 133 windows for each event A–D, resulting in $N \approx 4 \times 10^4$ FSM field measurements per window, along with 40 ion measurements and 200 electron measurements. The power spectrum of $\boldsymbol{B}$ in the spacecraft frame is given as $PSD(\boldsymbol{B}, k)$, where $k = 2\pi f/v_0$, $v_0$ is the average flow speed in each region and $f$ is a discrete frequency increment in the range $N/f_s \leq f \leq f_s/2$. The transformation of frequency $f$ to wavenumber $k$ is performed assuming Taylor's hypothesis, which is discussed in-depth in Sec. II A. We calculate the trace power spectrum of the magnetic field, where components $B_{x,y,z}$ are pre-filtered with a Hanning window, and we take the sum of the power in the three components i.e., $P = \sum_i P(B_i)$.

In turbulent plasmas, the magnetic spectrum often appears as a series of power laws with varying indices, $P \propto k^{\alpha}$.[51] For example, power-law index $\alpha = -5/3$ corresponds to the inertial range of fluid turbulence,[52] typical of space plasmas at spatial scales far above ion kinetic scales. At the ion scales, $\sim d_i$ or $\sim \rho_i$, solar wind and magnetosheath plasmas typically exhibit a breakpoint below which the magnetic spectrum steepens. In this ion kinetic range, the power-law index $\alpha$ is variable, though $\alpha \approx -2.8$ is typical for the solar wind.[53,54] The breakpoint between the fluid MHD scale and the ion kinetic scale has been seen at the larger of $d_i$, or $\rho_i$[30] when observing solar wind undisturbed by the bow shock. A second breakpoint is often observed at electron kinetic scales, and again the slope of the magnetic spectrum is expected to steepen in the electron kinetic range, below $\sim d_e$. Hence, the magnetic spectrum is expected to comprise three or more distinct power laws with different slopes. To characterize the power laws of our observed magnetic spectra, we seek an algorithm that can generate and fit an arbitrary number of straight lines to a spectrum, with a variable number of breakpoints. Hence, we use the multivariate adaptive regression splines (MARS) algorithm, developed by Friedman,[55,56] and implemented by Milborrow *et al.*[57] This method produces a fit composed of piece-wise linear functions of the general form

$$\hat{f}(x) = \sum_{j=1}^{k} c_j B_j(x), \tag{9}$$

where $B_j$ are the basis functions implemented as hinge (sometimes called hockey-stick) functions, and $c_j$ are the coefficients. The fit is built iteratively using a forward pass—where knots are added to the fit and the fit quality is assessed—and a backwards pass—where the number of knots is reduced to account for overfitting. Additionally, the MMS noise floor was found to be reached at wavenumbers of approximately $k \approx 10\,\mathrm{km}^{-1}$; therefore, the spectra at $k \geq 10\,\mathrm{km}^{-1}$ has been excluded from the MARS fit. This was found to significantly reduce the effect of the noise floor, although it does appear in some windows as spectral indices $\geq 0$ at the largest $k$.

Figure 3 shows an example of a spectrum obtained when MMS was downstream of the shock during event A, with the resultant MARS fit overlaid. Examples from the solar wind and magnetosheath and for event D can be found in Fig. S2 in the supplementary material. We also note that an electron scale wave is visible at $k \approx 2\,\mathrm{km}^{-1}$ as a peak in the spectrum. Similar structures appear in other intervals and are characterized by a dramatic change from positive to negative power law index at the electron scale. This demonstrates that the MARS method is able to identify spectral features associated with wave activity and allow interpretation of them separately from the background turbulent spectrum.

Figures 4 and 5 show the evolution of spectral index with time for the intervals A and D, respectively. Equivalent plots are given for events B and C in Figs. S3 and S4 in the supplementary material. Each 6 s window is represented as a vertical slice where the spectral index at a given scale is represented by the color of the vertical bar. The extent in $k$ over which that scale applies is given by the height of the bar, with each slice in time usually having three or more distinct slopes covering the observed spectrum.

In Fig. 4, we see that in the solar wind immediately preceding the shock, the breakpoint (BP) between the inertial (MHD) range and the ion (kinetic) range is at $k_{BP} \gg 1/d_i$. As in Fig. 3, this observation differs from studies, e.g., Ref. 30, who suggest that in undisturbed solar wind, the spectral break should be $d_i$ or greater. However, in the magnetosheath close to the shock, we find that the breakpoint shifts to larger scales and settles much closer to $d_i$. This is most likely due to the lack of clean, undisturbed solar wind very close to the bow shock.

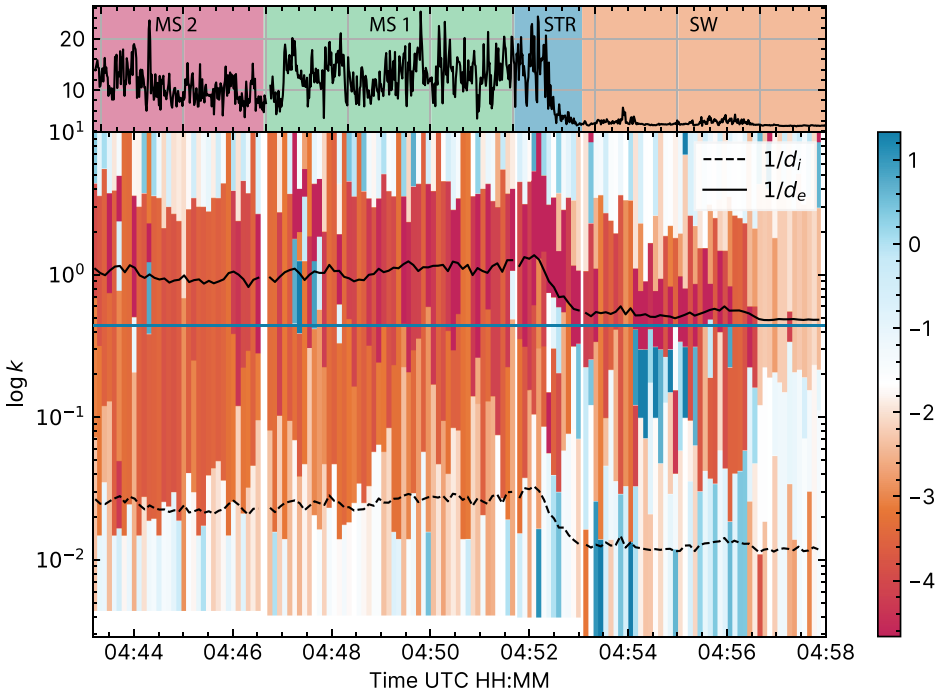


**FIG. 4.** Evolution of spectral slopes as a function of time for event A. Top: magnetic field strength, $|\boldsymbol{B}|$. Colors refer to magnetosheath (MS 1/2), shock transition region (STR), and solar wind (SW). Bottom: evolution of spectral indices from MARS fit. Note that this does not always split the spectrum into three regions. The color represents the slope of the power-law fit. Red indicates steeper than $-5/3$, while blue is shallower than $-5/3$. Breakpoints are indicated by a change in color. Electron scales, $\rho_e \approx d_e$ are shown as a solid black line, and the ion scale $d_i$ is shown as a dashed black lines. For wavenumbers much greater than the blue horizontal line, whistler waves will begin to violate Taylor's hypothesis. Event A is a quasi-perpendicular shock and as a result we get a clear distinction between solar wind and magnetosheath spectra. The ion-inertial breakpoint (BP) is $1/d_i > k > 1/\rho_i$ in the magnetosheath.

For event D, Fig. 5, the spectral slope in the solar wind is much steeper than expected at spatial scales larger than the ion inertial length, with $\alpha \sim -4$ on average. This feature may be caused by an upstream wave for which the peak wavelength is greater than the maximum resolvable within each 6 s window. Alternatively, short-sample effects such as a localized shear or other sporadic and discontinuous event could also cause a steepening of the spectral slope when measured using 6 s windows. This steep spectral slope is not observed

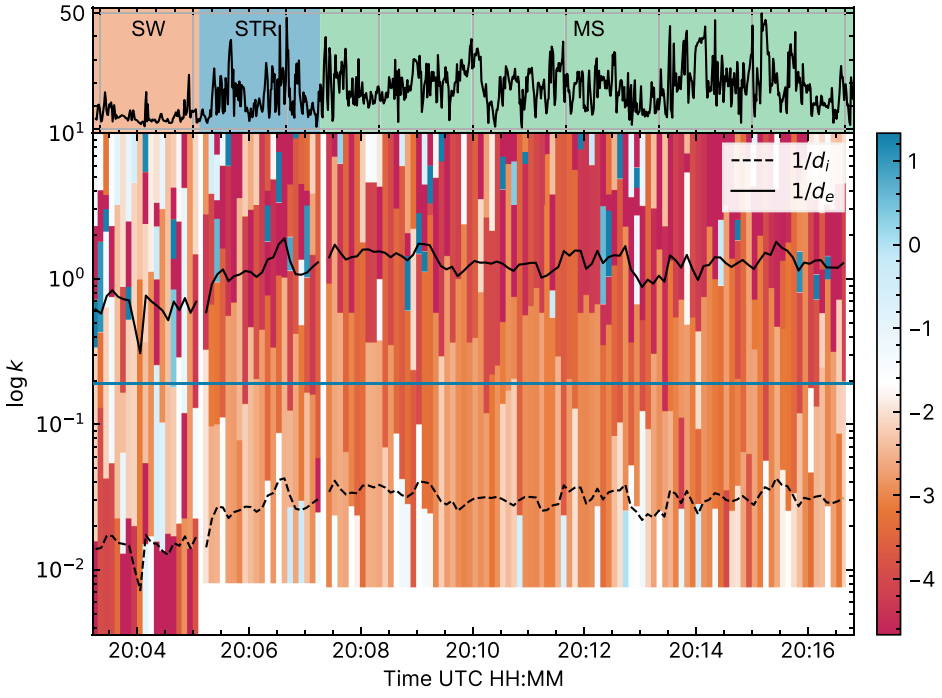


**FIG. 5.** Equivalent to Fig. 4 for interval D, 20 March 2020. There are many windows where the breakpoint is aligned with $1/d_i$ throughout the whole event. In the magnetosheath the breakpoints move from shallower to steeper with increasing $k$, but in the solar wind the opposite is true and the spectrum is steeper when $k < 1/d_i$.

in the shock transition or magnetosheath. Downstream of the shock, the breakpoint between inertial and ion scales tracks well with $d_i$ for most windows. In the inertial range, we observe a steady spectral slope of $\alpha \sim -5/3$ approximately 1 min after the spacecraft crosses the shock ramp.

Figure 6 shows the average slope as a function of scale, $k$, for intervals A and D, broken down into subsections based on MMS's location in relation to the shock, e.g., magnetosheath (MS), in the shock transition region (STR) or the solar wind (SW). The chosen intervals corresponding to each region are shown in the top panels of Figs. 4 and 5. Similar figures for intervals B and C are given in Figs. S5 and S6 in the supplementary material. Errors shown are sample standard deviations from all windows within the region. For a "quiet" boundary layer that introduces no new fluctuations to the medium, and instead is simply a superposition of modes either side, we might expect the spectral slope within that boundary to be between the slope either side. For such a shock, the slope in the STR would be between those in the SW and MS at all scales. That is, we would see the blue line (slope in the STR) between the green (MS) and yellow (SW) lines at all scales, as this would indicate that it is purely a transitional state as solar wind plasma crosses the shock and into the magnetosheath. However, we expect the shock to introduce new waves and instabilities. This is apparent for the given events where the STR slope is outside of the MS and SW lines. In event A, we see this most prominently at electron scales ($k \approx d_e$), whereas for event D, this occurs at $k \approx 3d_e$. As has been discussed in Sec. II A 1, spectral slopes at electron scales may be affected by the influence of whistler waves on the validity of Taylor's hypothesis; however, simulations (e.g., by Howes *et al.*[46]) suggest this results in shallower slopes, not steeper, as observed here. We also note the extremely steep slope in the inertial range for the solar wind in event D, which was also visible in Fig. 5. However, for most scales, the shock transition region lies between the SW and MS lines, or very close to the MS. The source of the steeper shock transition region at electron scales could be due to similar scale instabilities or other non-turbulent fluctuations at the shock, or an indication of a more efficient turbulent energy dissipation process.

The slopes of MARS fits to each entire region (MS, STR, and SW) can also be seen in Fig. 6. These regions are significantly longer in duration (∼minutes) than the 6 s windows and are, therefore, much less sensitive to short-sample effects. The local (6 s) average slopes

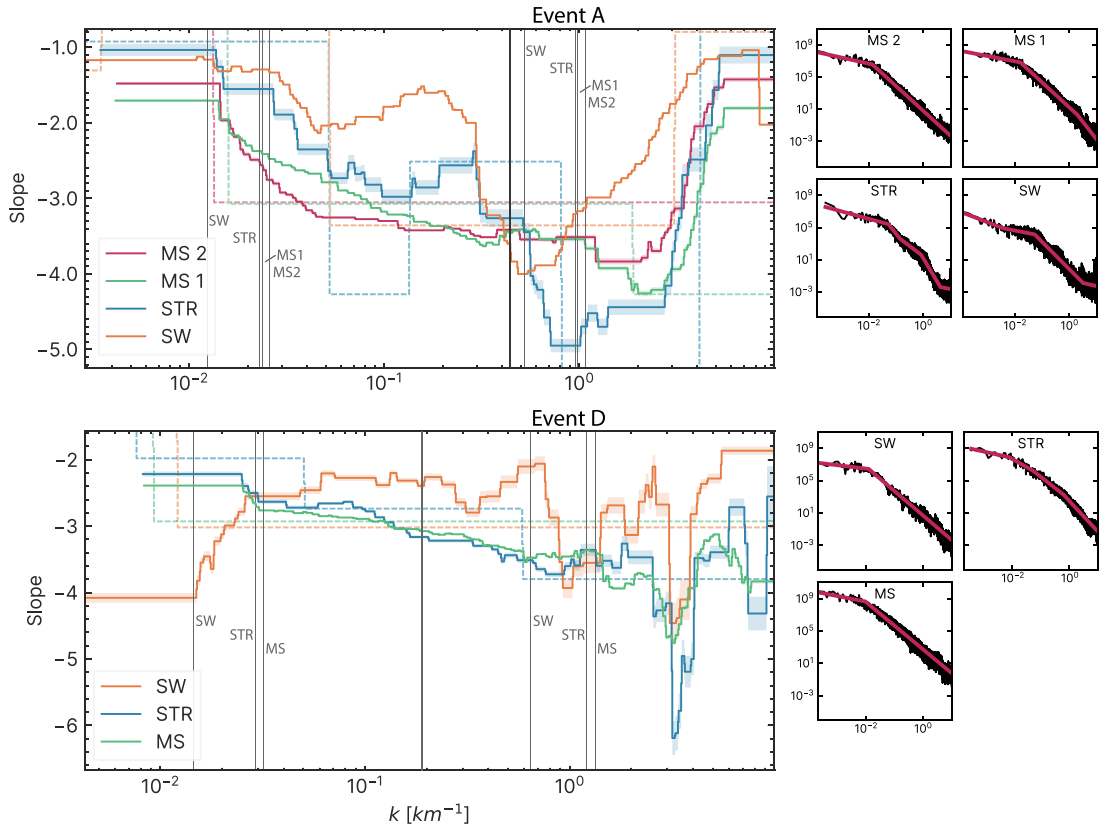


**FIG. 6.** Step plots of average slope as a function of scale for event A (quasi-perpendicular), top, and event D (quasi-parallel), bottom. In the main (left) panels, each colored line represents a subsection of the entire interval, i.e., magnetosheath (MS—red or green), the shock transition region (STR—blue), or solar wind (SW—orange). The "MS 2" line is further downstream than "MS 1." See Figs. 4 and 5 for a definition of the boundaries. Average kinetic scales, $d_i \approx 10^{-2}$ and $d_e \approx 10^{0}$, are also plotted as vertical black lines, labeled with the corresponding region. The scale where whistler waves may begin to violate Taylor's hypothesis is shown by bold vertical black line. We see that there are occasions in both panels where the STR spectral index lies outside of the transition between SW and MS. The clusters of panels on the right are the magnetic spectra of each entire interval. The red lines show the MARS fit to this "region average," which are also shown as colored dashed lines in the main panels.

track the behavior of the region average in general, with the exception of scales $k < 10^{-2}$ in the solar wind in event D. This shows that, in the areas discussed here, the evaluation of spectral power is not significantly affected by local shears.

Comparing the average slopes in Fig. 6 to recent statistics from Ref. 58 of the magnetosheath close to the bow shock at MHD and sub-ion scales, we find that event A compares well in both regions, and event D agrees with statistics in the sub-ion range. In event A, the slope in the MHD range is $\sim -1.7$, compared to $-1.47 \pm 0.24$ found by Li *et al.*[58] for quasi-perpendicular shocks. In the sub-ion range, the slope is $\sim -3.3$ at the midpoint between $\rho_i$ and $\rho_e$, compared to $-2.97 \pm 0.65$. For event D, the MHD slope is $\sim -2.2$ compared to $-1.46 \pm 0.38$, while for sub-ion scales, the slope is $\sim -3.1$ at the midpoint, compared to $-2.84 \pm 0.15$ from Ref. 58. This shows that event A is a more "typical" quasi-perpendicular shock while event D has steeper slopes at both MHD and sub-ion scales than might be expected for a typical quasi-parallel shock.

## IV. KURTOSIS

A fundamental method for studying intermittency is to examine deviations from Gaussianity in the distribution of magnetic field fluctuations, for which a typical method is to use the kurtosis.[59] Intermittency is associated with strong, highly localized gradients, especially at small scales. If the kurtosis $\kappa(\boldsymbol{B}) > 3$, then the magnetic field has an overabundance of extreme gradients relative to a normal distribution, which therefore indicates the existence of intermittent (or self-similar) structures. $\kappa \leq 3$ indicates that strong, localized gradients are not present.

Here, we use the standard definition of kurtosis as a numerical summary measure, from Ref. 60,

$$\kappa = m_4/m_2^2, \tag{10}$$

where

$$m_r = \frac{1}{n}\sum_{i=1}^{n}(x_i - \bar{x})^r, \tag{11}$$

where $m_r$ is the $r$th moment about the mean, $n$ is the length of the data, $x_i$ is the $i$th observation and $\bar{x}$ is the arithmetic mean of the observations.

Figure 7, panels (a) and (d), show the kurtosis, independent of scale, for events A and D. Events B and C are shown in Figs. S7 and S8 in the supplementary material. The kurtosis is calculated for consecutive windows containing $10^5$ samples, based on the rule of thumb $m_{\max} = \log N - 1$, where $m_{\max}$ is the maximum moment (i.e., fourth) and $N$ is the number of samples.[61] Considering the FSM cadence of 1/8192 s, this corresponds to 12.2 s per window. In event A, we see a clear difference in kurtosis between the solar wind and magnetosheath. Strong, small-scale gradients associated with high kurtosis are present upstream of the shock, but there are very few occasions where $\kappa > 3$ in the downstream. The kurtosis peaks to over 20 as the spacecraft crosses the shock ramp into the solar wind in event A. In event D, we see the kurtosis peaking in the solar wind before the shock transition region, but the peak is much lower at ~7, about one third of the peak in event A. Following the shock there is a period of Gaussian kurtosis ($\kappa \sim 3$), and even some times where the distribution is platykurtic ($\kappa < 3$). However, the kurtosis does begin to increase again further into the magnetosheath. This could be due to motion of the shock front toward the spacecraft, causing a partial crossing.

To directly compare the prevalence of high kurtosis fluctuations across the shock, we next examine the difference between the proportion of bins with $\kappa > 3$. For event A, we find that there is a large change across the shock: In the solar wind 60.7% of bins show signs of high kurtosis fluctuations, whereas 31.8% of bins do in the magnetosheath. For quasi-parallel event D we observe a lower proportion of high kurtosis intervals in the upstream, with 50.0% in the solar wind, and a similar proportion to event A, 31.4%, in the magnetosheath.

Therefore, in comparing the kurtosis observed in quasi-parallel and quasi-perpendicular shocks, we find that there are significant changes between the upstream and downstream distributions. The solar wind close to the shock and the shock foot has significantly higher kurtosis than the magnetosheath. This is visible in both the quasi-parallel and quasi-perpendicular case. However, the peak kurtosis is significantly higher for the quasi-perpendicular event by a factor of approximately three. The higher kurtosis in the SW, particularly in event A, is likely influenced by high kurtosis specifically at scales approaching the inertial range. Therefore, we now look at the scale dependence of the kurtosis.

Intermittency is more strictly defined as also requiring a relationship with scale, where shorter scales should have a high kurtosis ($\kappa > 3$), but at longer scales (fluctuations $\gg d_i$) kurtosis will decrease as the signal begins to appear self-similar.[51] Hence, we also show the scale-dependent kurtosis $\kappa_S(\ell) = S_4(\ell)/S_2(\ell)^2$ in Fig. 7, panels (b) and (e). The equation for structure function, $S_N$ of order $N$ is

$$S_N(\ell) = \left\langle \sum_{i=x,y,z} \delta B_i(x,\ell)^N \right\rangle_X, \tag{12}$$

where

$$\delta B_i(x,\ell) = B_i(x+\ell) - B_i(x), \tag{13}$$

and $\ell$ is the lag in kilometers, obtained through the Taylor hypothesis, and $\langle\rangle_X$ represents an average across all points in the interval. In Fig. 7, panels (c) and (f), we show the resultant estimated slope of a power law fit to $\log(\kappa_S) \propto \log(\ell)$. A steeper (more negative) slope is associated with a stronger scaling relation, which suggests stronger intermittency. From this, we see event A [panels (b) and (c)] that the dependence of $\kappa_S$ on $\ell$ is stronger in the magnetosheath than in the solar wind or shock transition. In event D [panels (e) and (f)], the scaling is strongest in the shock transition, but is still overall comparable to the magnetosheath in event A.

## V. CORRELATION LENGTH

Next, we seek to measure a characteristic size of turbulent fluctuations in the magnetic field. Energy is typically transferred in a "cascade" from large to small scales on average, generating magnetic structures at sizes ranging from stirring scales to the scales at which energy is dissipated. The correlation length, $\lambda_c$, quantifies the average size of the largest scale fluctuations visible in the data,[29,45] which can be associated with the "stirring" scale, providing the dataset covers a portion of space significant enough for large correlation lengths to be observed, i.e., a window where MMS travels a distance through the plasma in the plasma rest frame that is comparable to or larger than the correlation scale. The autocorrelation function of magnetic fluctuations is given by

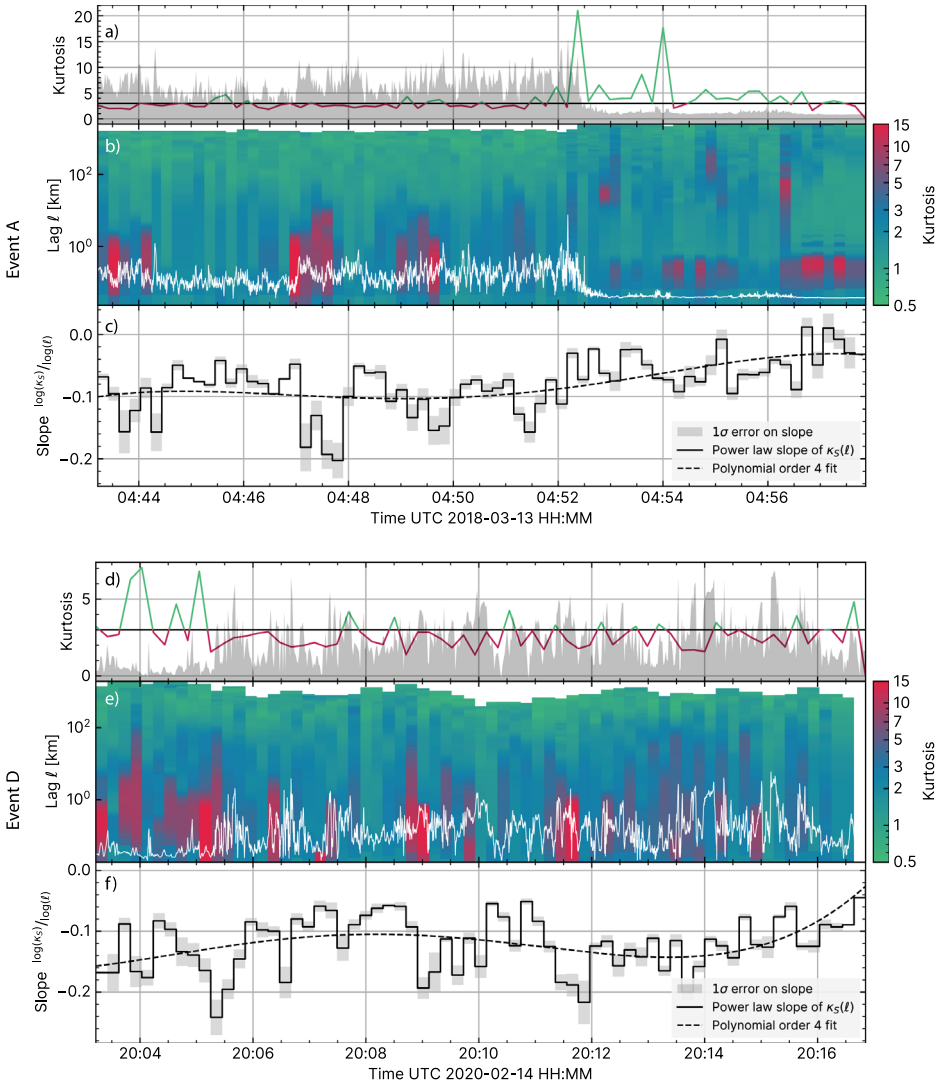


**FIG. 7.** Kurtosis examined for events A (top group) and D (bottom group). (a) and (d) Scale-independent kurtosis, $\kappa > 3$ is shown green, and $\kappa \leq 3$ is red. A horizontal black line highlights $\kappa = 3$. $|\boldsymbol{B}|$ is displayed for reference as a gray shaded background. The quasi-perpendicular event A shows a clear difference between solar wind and magnetosheath, with $\kappa$ peaking in the shock foot. The quasi-parallel example (event D) shows a similar relationship, however toward the end of the interval $\kappa$ begins increasing again. (b) and (e) Scale-dependent kurtosis, each column shows kurtosis as a function of scale (lag $\ell$ in km, vertical axis). We show $|\boldsymbol{B}|$ in white for comparison. Intervals containing missing data are shown as white. (c) and (f) Power law index (black line), $m$, of a linear fit to $\log(\kappa_S) = m\log(\ell) + C$, where $C$ is constant. The $1\sigma$ standard deviation on the estimated slope is shown as a gray shaded region. We also fit a fourth order polynomial to these slopes (dashed line) as a visual aid. A steeper (i.e., more negative) slope is associated with a stronger scaling relation.

$$R(l) \equiv \frac{\langle \mathrm{Tr}[\delta\boldsymbol{b}(\boldsymbol{x}+l)\delta\boldsymbol{b}(\boldsymbol{x})]\rangle}{\langle|\delta\boldsymbol{b}|^2\rangle}. \tag{14}$$

We define the correlation length as follows:

$$\lambda_c \equiv \int_0^\infty R(l)\, dl, \tag{15}$$

where Tr[…] is the trace, $\delta\boldsymbol{b} \equiv \boldsymbol{B} - \langle\boldsymbol{B}\rangle$, and $l$ is the lag of the autocorrelation. This calculation is achieved by integration up to the first zero crossing of $R(l)$, or by a fit of the form $R(l) \propto \exp(-l/\lambda_c)$. We find that results do not differ significantly between methods, and therefore, we present results using the integration method.

Correlation length generally relies on having a data set long enough for a correlation function to become uncorrelated. However, the region of space near the bow shock is a rapidly changing environment dominated by processes unrelated to turbulence. Care is, therefore, needed when selecting what scale of fluctuations should be included. Since the shock amplitude is significantly larger than any turbulent fluctuation (particularly in quasi-perpendicular shocks), then any window of time that includes the shock will have a correlation length that is closely related to the crossing time of the shock, since it will dominate the autocorrelation function.

In this case, it is more descriptive to examine fluctuations at scales smaller than the step-function introduced to the time series by the shock. Therefore, we use a variable high-pass filter over the event to remove the effect of low frequency variations, such as the shock ramp. A 10th order Butterworth filter was used, which can be defined by the critical frequency, $F_{\mathrm{crit}} \equiv 1/T_{\mathrm{max}}$ where $T_{\mathrm{max}}$ is the longest time allowed by the filter. By varying $T_{\mathrm{max}}$, the data are limited exclusively to fluctuations with wavelength shorter than $v_0/2F_{\mathrm{crit}}$. If $T_{\mathrm{max}}$ is less than the period associated with the stirring scale of the turbulence, then the measured $\lambda_c$ will have a dependence on the size of the filter, increasing in proportion to $T_{\mathrm{max}}$. When $T_{\mathrm{max}}$ becomes greater than the period associated with the stirring scale, $\lambda_c$ will appear to plateau,

and changes in $T_{max}$ will not have a significant effect on $\lambda_c$. Filtering $\lambda_c$ in this manner provides information on coherence scales at, crucially, scales $\leq T_{max}$. i.e., With this method we do not capture coherence at large scales, most notably in the solar wind. However, in the bow shock and magnetosheath, as well as in foreshock structures, we find that this method works well, since $\lambda_c \leq T_{max}$ in these regions.

Similar to the approach used when discussing the magnetic spectrum, we have split the interval into smaller consecutive windows. The range of $T_{max}$ was chosen to cover several decades in duration and is approximately logarithmically spaced. The entire event is filtered according to $T_{max}$ before being split into windows. Figure 8 describes the evolution of the frequency-dependent correlation length for event A. Plateaus—areas without a significant change in color between adjacent $T_{max}$ bins—indicate that a consistent correlation length has been reached. We see that in the solar wind, a consistent $\lambda_c$ is not reached; the maximum observed correlation length is over $100d_i$. However, if burst data were available further into the solar wind, we would likely have seen this increase far higher, given that solar wind correlation lengths have been measured by the ACE spacecraft at the L1 Lagrange point to be $0.03–0.08AU$, which is approximately $50–100 \times 10^3 d_i$.[62] In the magnetosheath, we see a very clear plateau of $3–10d_i$ immediately downstream of the shock, which appears to slowly increase further into the magnetosheath. At the point in the magnetosheath furthest from the shock (04:42), the correlation length may still be in a plateau but with $\lambda_c > 10d_i$.

Figure 9 shows an equivalent plot for the quasi-parallel event, D. The correlation length on the SW side is approximately $\lambda_c = 3–10d_i$. There is a foreshock structure at 20:04 UTC which may be a partial shock crossing. This indicates that this may not be representative of the solar wind and is instead an extended shock transition region or foreshock. These structures may reduce the average correlation length, similar to Fig. 8. The correlation length after the shock also appears to be in the range $\lambda_c = 10–12d_i$, approximately the same as what is observed for the quasi-perpendicular event A. These correlation lengths can be compared to recent results of Stawarz *et al.*,[45] who found that $\lambda_c \approx 10$ s of $d_i$ at the sub solar magnetosheath, gradually increasing to hundreds of $d_i$ in the flanks. For the shocks analyzed here, MMS entered the sheath in or close to the sub solar region, and therefore, our results are consistent.

Finally, there are indications that shock micro-structure and non-stationarity may also have an effect on the correlation length. In the quasi-perpendicular case, Fig. 8, we see two periods of upstream wave activity visible at 04:54 and 04:56 in the top panel, both approximately 60 s in duration. This causes a significant reduction of $\lambda_c$ of approximately a factor of 10 compared to the immediate surroundings, but only for $T_{max} \leq 60$ s. Similar structure is also visible to a lesser extent within the shock ramp at 04:52:30. These upstream wave packets may be partial crossings of the shock foot caused by ripples on the shock surface.[63] Hence, the features in the filtered correlation length may be associated with fluctuations in the foot and ramp arising from this form of non-stationarity. They also appear at larger scales (longer $T_{max}$) further from the shock, and smaller scales (shorter $T_{max}$) closer to the shock, which is perhaps evidence of structures transitioning from larger to smaller scales as the solar wind plasma approaches the shock. A similar effect is visible in Fig. 9, where periods of large magnetic field amplitude are associated with lower correlation length than the surroundings. However, they are shorter in duration, and we do not observe a reduction in correlation length closer to the shock. The occurrence of these structures would suggest the presence of narrow band waves generated in the shock transition region. However, since $\lambda_c$ depends on Taylor's hypothesis and this micro-structure is seen at very small correlation lengths, it is important to note that it

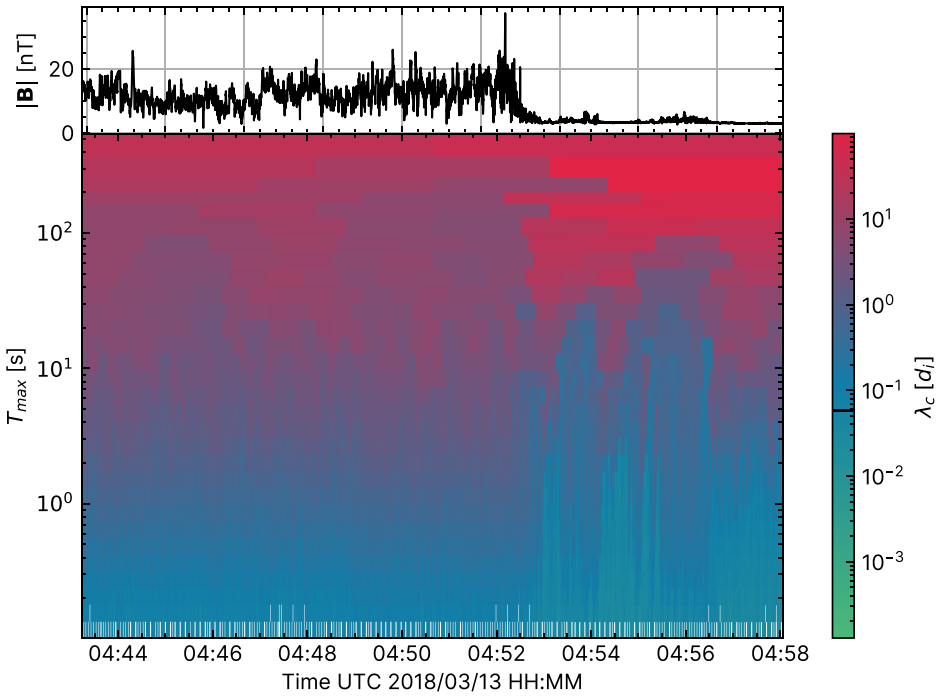


**FIG. 8.** Upper: magnetic field strength, $|B|$. Lower: correlation length, $\lambda_c$, color (units of ion inertial length), as a function of time and $T_{max}$. The width of each bin is equal to $T_{max}$ up to $T_{max}$ = total interval length/2. The black line on the color bar at $\lambda_c = 5.91 \times 10^{-2}$ indicates the scale at which whistler waves may begin to influence the accuracy of Taylor's hypothesis. A plateau, which can be seen in areas where the color ($\lambda_c$) does not change significantly when moving up to a larger $T_{max}$, indicates that the fluctuations are correlated on scales equal-to or smaller-than $T_{max}$. There is an observable difference in $\lambda_c$ before and after the shock; a large plateau exists between $\lambda_c = 3$ and 10 immediately downstream of the shock, but in the region upstream of the shock transition region $\lambda_c$ exceeds $100d_i$.

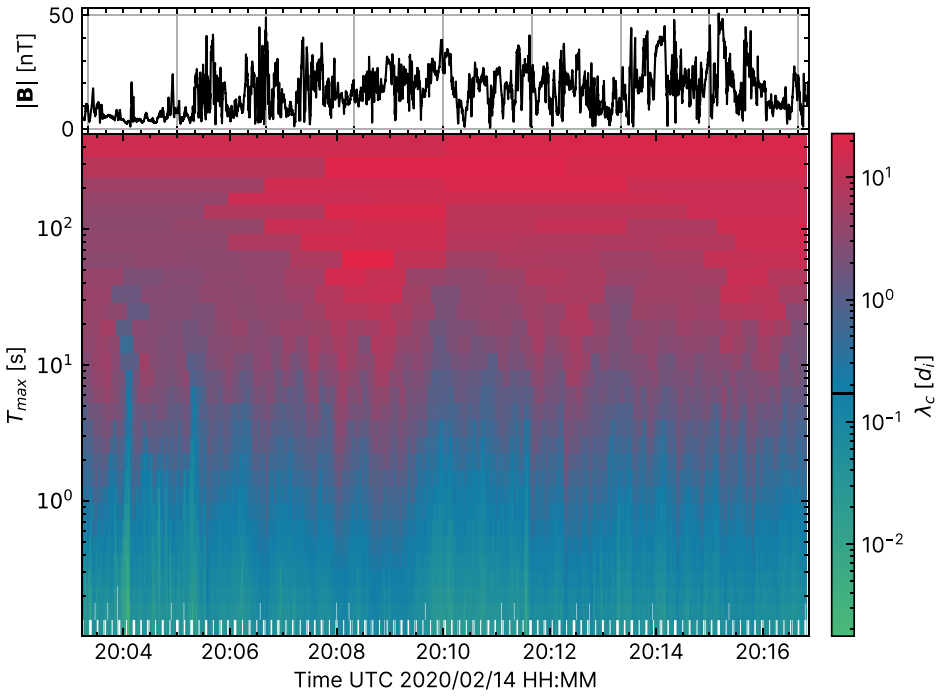


**FIG. 9.** Similar to Fig. 8 for event D. In this event, correlation length appears to increase on the magnetosheath side. The whistler wave limit for Taylor's hypothesis is at $\lambda_c = 0.17$.

may also be affected by the presence of whistler waves, which would act to increase $\lambda_c$.

## VI. CONCLUSIONS

In this study, we used three different measures of turbulence—the magnetic spectrum, scale-independent kurtosis, and correlation length—to explore the evolution of the solar wind and magnetosheath turbulence across Earth's bow shock. The influence of the bow shock transition region on the properties of turbulence is not currently well understood. Therefore, by using the magnetic spectrum to observe differences in the turbulent energy cascade, the kurtosis to explore the properties of intermittency and the correlation length to describe changes in coherence scales, we aim to produce a representative picture of how turbulence evolves from the solar wind, across the bow shock, and downstream into the magnetosheath. We, therefore, address the following questions: (1) Is there a measurable difference between turbulence seen in the bow shock transition region and in the surrounding plasma? (2) How quickly does well-developed turbulence arise in the magnetosheath after a bow shock crossing?

We find that the shock transition region displays features in the spacecraft frame magnetic spectrum that are different from the turbulence present in the solar wind and magnetosheath. This can be seen as shock transition spectral slopes which are much steeper at scales where $k \geq d_e$ than either of their upstream or downstream neighbors (Fig. 6). This suggests shock processes are driving scale-dependent energy dissipation at sub-electron scales. This is observed at both quasi-parallel and quasi-perpendicular shocks (events A and D, $\theta_{Bn} = 68°$ and 33°, respectively). However, we note that these signatures are not always so clearly observable, which is the case for events B and C. Figures showing structure (or lack thereof) in the magnetic spectral indices and scale-independent kurtosis are shown for events B and C in the supplementary material. We find that the breakpoint ($BP$) separating the inertial range from the ion range transitions from $BP \ll d_i$ before the shock, to $d_i \leq BP \leq \rho_i$ in the magnetosheath.

Finally, we have adapted the definition of correlation length to include a high-pass filter defined by a critical frequency $F_{\text{crit}}$, which allowed us to calculate a turbulent correlation length across the shock that effectively removes the large-scale spectral influence of the shock. We found that close to the shock the correlation length is longer on the solar wind side than the magnetosheath side. Plateaus in high-pass filtered correlation length averaged $25d_i$ in the solar wind and $<20d_i$ in the magnetosheath. This relates to a reduction in size of the stirring scale in the magnetosheath when compared to solar wind close to the shock. We found that upstream structures in the shock transition region introduce plateaus of reduced correlation length for short periods of time, on the order of tens of seconds.

The magnetic spectrum transitioned from solar wind-like to magnetosheath-like over a 20 s interval for event A and a 1 min interval for event D. This corresponds to $180d_i$ and $1.1R_E$ for event A and $600d_i$ $3.1R_E$ for event D. Additionally, the intermittency (kurtosis $\kappa > 3$) seen in the upstream transitioned to the average magnetosheath (non-intermittent) level after 30 s ($267d_i$ or $1.7R_E$) in the quasi-perpendicular case, whereas for the quasi-parallel shock, intermittency was still present until two minutes ($1.2 \times 10^3 d_i$ or $6.2R_E$) after the shock crossing. With regard to the correlation length, the quasi-perpendicular case demonstrated a rapid (~6 s) transition from solar wind-like scales to magnetosheath-like scales on crossing the shock ramp. In the quasi-parallel case, however, the transition was much slower, occurring over a period of approximately 2 min. Together, these results suggest that the time needed for the turbulent fluctuations to fully develop after crossing the shock ramp is dependent on $\theta_{Bn}$.

Since the majority of observations discussed here have made use of Taylor's hypothesis,[40] we have also discussed in-depth the limitations this method introduces to the interpretation of results. In particular those at electron kinetic scales, where whistler-mode waves can affect the assumptions underpinning the use of Taylor's hypothesis in transforming single-spacecraft time series observations into the spatial frame. This is discussed in Sec. II A.

Although it is not possible to describe in detail the nature of the physical processes in the transition region from just the turbulence measures presented here, we can present general characteristics of some quasi-parallel and quasi-perpendicular structures. Current sheets, which appear most prominently downstream of the quasi-parallel shock, are expected to cause a steepening of the power spectrum near the current sheet scale due to dissipation by magnetic reconnection, where more current sheets is suggested to result in greater steepening.[29] These structures are also associated with an increase in kurtosis, but little change in the correlation length, $\lambda_c$. Large amplitude waves upstream of the quasi-parallel shock[64] are excited by reflected ions due to the ion beam instability. We suggest that they would cause an increase in power at around $1/d_i$ in the magnetic spectrum, thus steepening the spectral index at scales smaller than the wave scale. Similarly, high-amplitude wave packets may result in an increase in kurtosis and cause a plateau in $\lambda_c$ at the wave scale upstream of the shock. Ripples at the shock ramp[63] can be present for a large range of $\theta_{Bn}$, and can result in a steeper spectral index in the inertial or ion ranges, depending on their wavelengths. As with other wave-like structures, they may cause an increase in kurtosis, and a plateau in $\lambda_c$ at the shock ramp. Similarly, ion cyclotron[65] and mirror mode waves,[66–68] which can both occur at quasi-perpendicular shocks, may increase the power in the magnetic spectrum at the wave scale, increase kurtosis, and, if the wave is the dominant structure, result in a plateau in $\lambda_c$ at the wave scale.

We note that the case studies shown here may not be representative of all shocks. For example, as discussed earlier, the four events detailed here are all for slow solar wind. The natural next step is, therefore, to determine whether the conclusions reached here are representative of the typical quasi-parallel or quasi-perpendicular shock. In a future work, we will compile a statistical survey of shocks across a range of shock normal angles and other plasma parameters, to explore the average behavior of the bow shock. Additionally, we will explore the applicability of these methods to simulations.

## SUPPLEMENTARY MATERIAL

See the supplementary material for additional Figs. S1–S8, which show tests of Taylor's hypothesis for events B and C; examples of the magnetic spectrum for events A and D; and the evolution of the spectral index fits, average spectral index, and kurtosis for events B and C. These figures are referenced throughout the main text of the article as required.

## ACKNOWLEDGMENTS

J. Plank was supported by STFC studentship ST/V507064/1 (Grant No. 2502298). I.L. Gingell was supported by the Royal Society University Research Fellowship via No. URF\R1\191547.

## AUTHOR DECLARATIONS

### Conflict of Interest

The authors have no conflicts to disclose.

### Author Contributions

**James Plank:** Conceptualization (equal); Formal analysis (lead); Investigation (lead); Methodology (lead); Software (lead); Visualization (lead); Writing – original draft (lead); Writing – review & editing (lead). **Imogen L. Gingell:** Conceptualization (equal); Formal analysis (supporting); Funding acquisition (lead); Investigation (supporting); Methodology (supporting); Project administration (lead); Supervision (lead); Writing – review & editing (supporting).

## DATA AVAILABILITY

The data that support the findings of this study are openly available in the MMS Science Data Center at the Laboratory for Atmospheric and Space Physics (LASP) hosted by the University of Colorado, Boulder (https://lasp.colorado.edu/mms/sdc/public/), Refs. 32, 36, 69–71 and NASA/GSFC's Space Physics Data Facility's OMNIWeb service (https://omniweb.gsfc.nasa.gov/), Refs. 72–75.

## REFERENCES

[1]C. F. McKee and E. C. Ostriker, "Theory of star formation," Annu. Rev. Astron. Astrophys. **45**, 565–687 (2007).
[2]I. Zhuravleva, E. Churazov, A. A. Schekochihin, S. W. Allen, P. Arévalo, A. C. Fabian, W. R. Forman, J. S. Sanders, A. Simionescu, R. Sunyaev, A. Vikhlinin, and N. Werner, "Turbulent heating in galaxy clusters brightest in x-rays," Nature **515**, 85–87 (2014).
[3]A. Chasapis, W. H. Matthaeus, T. N. Parashar, M. Wan, C. C. Haggerty, C. J. Pollock, B. L. Giles, W. R. Paterson, J. Dorelli, D. J. Gershman, R. B. Torbert, C. T. Russell, P.-A. Lindqvist, Y. Khotyaintsev, T. E. Moore, R. E. Ergun, and J. L. Burch, "In situ observation of intermittent dissipation at kinetic scales in the Earth's magnetosheath," Astrophys. J. **856**, L19 (2018).
[4]O. Alexandrova, C. H. K. Chen, L. Sorriso-Valvo, T. S. Horbury, and S. D. Bale, "Solar wind turbulence and the role of ion instabilities," Space Sci. Rev. **178**, 101–139 (2013).
[5]R. Bruno and V. Carbone, "The solar wind as a turbulence laboratory," Living Rev. Sol. Phys. **10**, 2 (2013).
[6]K. H. Kiyani, K. T. Osman, and S. C. Chapman, "Dissipation and heating in solar wind turbulence: From the macro to the micro and back again," Philos. Trans. R. Soc., A **373**, 20140155 (2015).
[7]S. R. Cranmer, M. Asgari-Targhi, M. Paz Miralles, J. C. Raymond, L. Strachan, H. Tian, and L. N. Woolsey, "The role of turbulence in coronal heating and solar wind expansion," Philos. Trans. R. Soc., A **373**, 20140148 (2015).
[8]J. A. Klimchuk, "On solving the coronal heating problem," Sol. Phys. **234**, 41–77 (2006).
[9]V. Carbone, P. Veltri, and A. Mangeney, "Coherent structure formation and magnetic field line reconnection in magnetohydrodynamic turbulence," Phys. Fluids A **2**, 1487–1496 (1990).
[10]L. Franci, S. S. Cerri, F. Califano, S. Landi, E. Papini, A. Verdini, L. Matteini, F. Jenko, and P. Hellinger, "Magnetic reconnection as a driver for a sub-ion-scale cascade in plasma turbulence," Astrophys. J. **850**, L16 (2017).
[11]J. L. Burch, R. B. Torbert, T. D. Phan, L.-J. Chen, T. E. Moore, R. E. Ergun, J. P. Eastwood, D. J. Gershman, P. A. Cassak, M. R. Argall, S. Wang, M. Hesse, C. J. Pollock, B. L. Giles, R. Nakamura, B. H. Mauk, S. A. Fuselier, C. T. Russell, R. J. Strangeway, J. F. Drake, M. A. Shay, Y. V. Khotyaintsev, P.-A. Lindqvist, G. Marklund, F. D. Wilder, D. T. Young, K. Torkar, J. Goldstein, J. C. Dorelli, L. A. Avanov, M. Oka, D. N. Baker, A. N. Jaynes, K. A. Goodrich, I. J. Cohen, D. L. Turner, J. F. Fennell, J. B. Blake, J. Clemmons, M. Goldman, D. Newman, S. M. Petrinec, K. J. Trattner, B. Lavraud, P. H. Reiff, W. Baumjohann, W. Magnes,

M. Steller, W. Lewis, Y. Saito, V. Coffey, and M. Chandler, "Electron-scale measurements of magnetic reconnection in space," Science **352**, aaf2939 (2016).
[12]J. F. Drake, M. Swisdak, H. Che, and M. A. Shay, "Electron acceleration from contracting magnetic islands during reconnection," Nature **443**, 553–556 (2006).
[13]X. R. Fu, Q. M. Lu, and S. Wang, "The process of electron acceleration during collisionless magnetic reconnection," Phys. Plasmas **13**, 012309 (2006).
[14]Q. Lu, H. Wang, X. Wang, S. Lu, R. Wang, X. Gao, and S. Wang, "Turbulence-driven magnetic reconnection in the magnetosheath downstream of a quasi–parallel shock: A three-dimensional global hybrid simulation," Geophys. Res. Lett. **47**, e2019GL085661, https://doi.org/10.1029/2019GL085661 (2020).
[15]Q. Lu, Z. Yang, H. Wang, R. Wang, K. Huang, S. Lu, and S. Wang, "Two-dimensional particle-in-cell simulation of magnetic reconnection in the downstream of a quasi-perpendicular shock," Astrophys. J. **919**, 28 (2021).
[16]P. A. Isenberg and J. V. Hollweg, "On the preferential acceleration and heating of solar wind heavy ions," J. Geophys. Res. **88**, 3923, https://doi.org/10.1029/JA088iA05p03923 (1983).
[17]J. V. Hollweg, "Kinetic Alfvén wave revisited," J. Geophys. Res. **104**, 14811–14819, https://doi.org/10.1029/1998JA900132 (1999).
[18]T. D. Phan, J. P. Eastwood, M. A. Shay, J. F. Drake, B. U. O. Sonnerup, M. Fujimoto, P. A. Cassak, M. Øieroset, J. L. Burch, R. B. Torbert, A. C. Rager, J. C. Dorelli, D. J. Gershman, C. Pollock, P. S. Pyakurel, C. C. Haggerty, Y. Khotyaintsev, B. Lavraud, Y. Saito, M. Oka, R. E. Ergun, A. Retino, O. L. Contel, M. R. Argall, B. L. Giles, T. E. Moore, F. D. Wilder, R. J. Strangeway, C. T. Russell, P. A. Lindqvist, and W. Magnes, "Electron magnetic reconnection without ion coupling in Earth's turbulent magnetosheath," Nature **557**, 202–206 (2018).
[19]I. Gingell, S. J. Schwartz, J. P. Eastwood, J. L. Burch, R. E. Ergun, S. Fuselier, D. J. Gershman, B. L. Giles, Y. V. Khotyaintsev, B. Lavraud, P.-A. Lindqvist, W. R. Paterson, T. D. Phan, C. T. Russell, J. E. Stawarz, R. J. Strangeway, R. B. Torbert, and F. Wilder, "Observations of magnetic reconnection in the transition region of quasi-parallel shocks," Geophys. Res. Lett. **46**, 1177–1184, https://doi.org/10.1029/2018GL081804 (2019).
[20]R. Wang, Q. Lu, R. Nakamura, W. Baumjohann, C. T. Russell, J. L. Burch, R. E. Ergun, P. A. Lindqvist, S. Wang, B. Giles, and D. Gershman, "Interaction of magnetic flux ropes via magnetic reconnection observed at the magnetopause," J. Geophys. Res. **122**, 10436–10447, https://doi.org/10.1002/2017JA024482 (2017).
[21]N. Bessho, L.-J. Chen, S. Wang, M. Hesse, L. B. Wilson, and J. Ng, "Magnetic reconnection and kinetic waves generated in the Earth's quasi-parallel bow shock," Phys. Plasmas **27**, 092901 (2020).
[22]N. Bessho, L.-J. Chen, J. E. Stawarz, S. Wang, M. Hesse, L. B. Wilson, and J. Ng, "Strong reconnection electric fields in shock-driven turbulence," Phys. Plasmas **29**, 042304 (2022).
[23]I. Gingell, S. J. Schwartz, D. Burgess, A. Johlander, C. T. Russell, J. L. Burch, R. E. Ergun, S. Fuselier, D. J. Gershman, B. L. Giles, K. A. Goodrich, Y. V. Khotyaintsev, B. Lavraud, P.-A. Lindqvist, R. J. Strangeway, K. Trattner, R. B. Torbert, H. Wei, and F. Wilder, "MMS observations and hybrid simulations of surface ripples at a marginally quasi-parallel shock," J. Geophys. Res. **122**, 11003–11017, https://doi.org/10.1002/2017JA024538 (2017).
[24]Y. Matsumoto, T. Amano, T. N. Kato, and M. Hoshino, "Stochastic electron acceleration during spontaneous turbulent reconnection in a strong shock wave," Science **347**, 974–978 (2015).
[25]O. Alexandrova, "Solar wind vs magnetosheath turbulence and Alfvén vortices," Nonlinear Processes Geophys. **15**, 95–108 (2008).
[26]E. Yordanova, Z. Vörös, S. Raptis, and T. Karlsson, "Current sheet statistics in the magnetosheath," Front. Astron. Space Sci. **7**, 00002 (2020).
[27]S. Y. Huang, L. Z. Hadid, F. Sahraoui, Z. G. Yuan, and X. H. Deng, "On the existence of the Kolmogorov inertial range in the terrestrial magnetosheath turbulence," Astrophys. J. **836**, L10 (2017).
[28]F. Sahraoui, L. Hadid, and S. Huang, "Magnetohydrodynamic and kinetic scale turbulence in the near-Earth space plasmas: A (short) biased review," Rev. Mod. Plasma Phys. **4**, 4 (2020).
[29]J. E. Stawarz, J. P. Eastwood, T. D. Phan, I. L. Gingell, M. A. Shay, J. L. Burch, R. E. Ergun, B. L. Giles, D. J. Gershman, O. L. Contel, P.-A. Lindqvist, C. T. Russell, R. J. Strangeway, R. B. Torbert, M. R. Argall, D. Fischer, W. Magnes, and L. Franci, "Properties of the turbulence associated with electron-only magnetic reconnection in Earth's magnetosheath," Astrophys. J. **877**, L37 (2019).
[30]C. H. K. Chen, L. Leung, S. Boldyrev, B. A. Maruca, and S. D. Bale, "Ion-scale spectral break of solar wind turbulence at high and low beta," Geophys. Res. Lett. **41**, 8081–8088, https://doi.org/10.1002/2014GL062009 (2014).
[31]L. Franci, S. Landi, L. Matteini, A. Verdini, and P. Hellinger, "High-resolution hybrid simulations of kinetic plasma turbulence at proton scales," Astrophys. J. **812**, 21 (2015).
[32]J. L. Burch, T. E. Moore, R. B. Torbert, and B. L. Giles, "Magnetospheric multiscale overview and science objectives," Space Sci. Rev. **199**, 5–21 (2015).
[33]C. T. Russell, B. J. Anderson, W. Baumjohann, K. R. Bromund, D. Dearborn, D. Fischer, G. Le, H. K. Leinweber, D. Leneman, W. Magnes, J. D. Means, M. B. Moldwin, R. Nakamura, D. Pierce, F. Plaschke, K. M. Rowe, J. A. Slavin, R. J. Strangeway, R. Torbert, C. Hagen, I. Jernej, A. Valavanoglou, and I. Richter, "The magnetospheric multiscale magnetometers," Space Sci. Rev. **199**, 189–256 (2014).
[34]O. L. Contel, P. Leroy, A. Roux, C. Coillot, D. Alison, A. Bouabdellah, L. Mirioni, L. Meslier, A. Galic, M. C. Vassal, R. B. Torbert, J. Needell, D. Rau, I. Dors, R. E. Ergun, J. Westfall, D. Summers, J. Wallace, W. Magnes, A. Valavanoglou, G. Olsson, M. Chutter, J. Macri, S. Myers, S. Turco, J. Nolin, D. Bodet, K. Rowe, M. Tanguy, and B. de la Porte, "The search-coil magnetometer for MMS," Space Sci. Rev. **199**, 257–282 (2014).
[35]M. R. Argall, D. Fischer, O. L. Contel, L. Mirioni, R. B. Torbert, I. Dors, M. Chutter, J. Needell, R. Strangeway, W. Magnes, and C. T. Russell, "The fluxgate-searchcoil merged (fsm) magnetic field data product for mms," arXiv:1809.07388 (2018).
[36]C. Pollock, T. Moore, A. Jacques, J. Burch, U. Gliese, Y. Saito, T. Omoto, L. Avanov, A. Barrie, V. Coffey, J. Dorelli, D. Gershman, B. Giles, T. Rosnack, C. Salo, S. Yokota, M. Adrian, C. Aoustin, C. Auletti, S. Aung, V. Bigio, N. Cao, M. Chandler, D. Chornay, K. Christian, G. Clark, G. Collinson, T. Corris, A. D. L. Santos, R. Devlin, T. Diaz, T. Dickerson, C. Dickson, A. Diekmann, F. Diggs, C. Duncan, A. Figueroa-Vinas, C. Firman, M. Freeman, N. Galassi, K. Garcia, G. Goodhart, D. Guererro, J. Hageman, J. Hanley, E. Hemminger, M. Holland, M. Hutchins, T. James, W. Jones, S. Kreisler, J. Kujawski, V. Lavu, J. Lobell, E. LeCompte, A. Lukemire, E. MacDonald, A. Mariano, T. Mukai, K. Narayanan, Q. Nguyan, M. Onizuka, W. Paterson, S. Persyn, B. Piepgrass, F. Cheney, A. Rager, T. Raghuram, A. Ramil, L. Reichenthal, H. Rodriguez, J. Rouzaud, A. Rucker, Y. Saito, M. Samara, J.-A. Sauvaud, D. Schuster, M. Shappirio, K. Shelton, D. Sher, D. Smith, K. Smith, S. Smith, D. Steinfeld, R. Szymkiewicz, K. Tanimoto, J. Taylor, C. Tucker, K. Tull, A. Uhl, J. Vloet, P. Walpole, S. Weidner, D. White, G. Winkert, P.-S. Yeh, and M. Zeuch, "Fast plasma investigation for magnetospheric multiscale," Space Sci. Rev. **199**, 331–406 (2016).
[37]A. Lalti, Y. V. Khotyaintsev, A. P. Dimmock, A. Johlander, D. B. Graham, and V. Olshevsky, "A database of MMS bow shock crossings compiled using machine learning," J. Geophys. Res. **127**, e2022JA030454, https://doi.org/10.1029/2022JA030454 (2022).
[38]J. H. King, "Solar wind spatial scales in and comparisons of hourly wind and ACE plasma and magnetic field data," J. Geophys. Res. **110**, A02104, https://doi.org/10.1029/2004JA010649 (2005).
[39]M. Peredo, J. A. Slavin, E. Mazur, and S. A. Curtis, "Three-dimensional position and shape of the bow shock and their variation with Alfvénic, sonic and magnetosonic Mach numbers and interplanetary magnetic field orientation," J. Geophys. Res. **100**, 7907, https://doi.org/10.1029/94JA02545 (1995).
[40]G. I. Taylor, "The spectrum of turbulence," Proc. R. Soc. London, Ser. A **164**, 476–490 (1938).
[41]A. Chasapis, W. H. Matthaeus, T. N. Parashar, S. A. Fuselier, B. A. Maruca, T. D. Phan, J. L. Burch, T. E. Moore, C. J. Pollock, D. J. Gershman, R. B. Torbert, C. T. Russell, and R. J. Strangeway, "High-resolution statistics of solar wind turbulence at kinetic scales using the magnetospheric multiscale mission," Astrophys. J. **844**, L9 (2017).
[42]C. H. K. Chen and S. Boldyrev, "Nature of kinetic scale turbulence in the Earth's magnetosheath," Astrophys. J. **842**, 122 (2017).
[43]R. Chhiber, A. Chasapis, R. Bandyopadhyay, T. N. Parashar, W. H. Matthaeus, B. A. Maruca, T. E. Moore, J. L. Burch, R. B. Torbert, C. T. Russell, O. L. Contel, M. R. Argall, D. Fischer, L. Mirioni, R. J. Strangeway, C. J. Pollock, B. L. Giles, and D. J. Gershman, "Higher-order turbulence statistics in the Earth's magnetosheath and the solar wind using magnetospheric multiscale

observations," J. Geophys. Res. **123**, 9941–9954, https://doi.org/10.1029/2018JA025768 (2018).
[44]J. E. Stawarz, L. Matteini, T. N. Parashar, L. Franci, J. P. Eastwood, C. A. Gonzalez, I. L. Gingell, J. L. Burch, R. E. Ergun, N. Ahmadi, B. L. Giles, D. J. Gershman, O. L. Contel, P. Lindqvist, C. T. Russell, R. J. Strangeway, and R. B. Torbert, "Comparative analysis of the various generalized ohm's law terms in magnetosheath turbulence as observed by magnetospheric multiscale," J. Geophys. Res. **126**, 2020JA028447, https://doi.org/10.1029/2020JA028447 (2021).
[45]J. E. Stawarz, J. P. Eastwood, T. D. Phan, I. L. Gingell, P. S. Pyakurel, M. A. Shay, S. L. Robertson, C. T. Russell, and O. L. Contel, "Turbulence-driven magnetic reconnection and the magnetic correlation length: Observations from magnetospheric multiscale in Earth's magnetosheath," Phys. Plasmas **29**, 012302 (2022).
[46]G. G. Howes, K. G. Klein, and J. M. T. Barge, "Validity of the Taylor hypothesis for linear kinetic waves in the weakly collisional solar wind," Astrophys. J. **789**, 106 (2014).
[47]The necessary polarity analysis needed to distinguish between ion cyclotron and whistler waves has not been done here.
[48]S. Perri, S. Servidio, A. Vaivads, and F. Valentini, "Numerical study on the validity of the Taylor hypothesis in space plasmas," Astrophys. J., Suppl. Ser. **231**, 4 (2017).
[49]S. Y. Huang and F. Sahraoui, "Testing of the Taylor frozen-in-flow hypothesis at electron scales in the solar wind turbulence," Astrophys. J. **876**, 138 (2019).
[50]F. Sahraoui, G. Belmont, and M. L. Goldstein, "New insight into short-wavelength solar wind fluctuations from Vlasov theory," Astrophys. J. **748**, 100 (2012).
[51]U. Frisch, *Turbulence* (Cambridge University Press, 1995).
[52]A. N. Kolmogorov, "The local structure of turbulence in incompressible viscous fluid for very large Reynolds numbers," Proc. R. Soc. A: Math. Phys. Eng. Sci. **434**, 9–13 (1991).
[53]O. Alexandrova, J. Saur, C. Lacombe, A. Mangeney, J. Mitchell, S. J. Schwartz, and P. Robert, "Universality of solar-wind turbulent spectrum from MHD to electron scales," Phys. Rev. Lett. **103**, 165003 (2009).
[54]F. Sahraoui, M. L. Goldstein, G. Belmont, P. Canu, and L. Rezeau, "Three dimensional anisotropic k spectra of turbulence at subproton scales in the solar wind," Phys. Rev. Lett. **105**, 131101 (2010).
[55]J. H. Friedman, "Multivariate adaptive regression splines," Ann. Stat. **19**, 1–67 (1991).
[56]J. J. Faraway, *Extending the Linear Model with R* (Chapman and Hall/CRC, 2016).
[57]S. Milborrow, T. Hastie, and R. Tibshirani, *Earth: Multivariate Adaptive Regression Splines* (2011).
[58]H. Li, W. Jiang, C. Wang, D. Verscharen, C. Zeng, C. T. Russell, B. Giles, and J. L. Burch, "Evolution of the Earth's magnetosheath turbulence: A statistical study based on MMS observations," Astrophys. J. **898**, L43 (2020).
[59]W. H. Matthaeus, M. Wan, S. Servidio, A. Greco, K. T. Osman, S. Oughton, and P. Dmitruk, "Intermittency, nonlinear dynamics and dissipation in the solar wind and astrophysical plasmas," Philos. Trans. R. Soc., A **373**, 20140154 (2015).
[60]S. Kokoska and D. Zwillinger, *CRC Standard Probability and Statistics Tables and Formulae, Student Edition* (CRC Press, 2000).
[61]T. Dudok de Wit, O. Alexandrova, I. Furno, L. Sorriso-Valvo, and G. Zimbardo, "Methods for characterising microphysical processes in plasmas," Space Sci. Rev. **178**, 665–693 (2013).
[62]B. R. Ragot, "Solar wind magnetic field correlation length: Correlation functions versus cross-field displacement diffusivity test," Astrophys. J. **927**, 182 (2022).
[63]A. Johlander, S. Schwartz, A. Vaivads, Y. V. Khotyaintsev, I. Gingell, I. Peng, S. Markidis, P.-A. Lindqvist, R. Ergun, G. Marklund, F. Plaschke, W. Magnes, R. Strangeway, C. Russell, H. Wei, R. Torbert, W. Paterson, D. Gershman, J. Dorelli, L. Avanov, B. Lavraud, Y. Saito, B. Giles, C. Pollock, and J. Burch, "Rippled quasiperpendicular shock observed by the magnetospheric multiscale spacecraft," Phys. Rev. Lett. **117**, 165101 (2016).
[64]E. A. Lucek, T. S. Horbury, A. Balogh, I. Dandouras, and H. Rème, "Cluster observations of structures at quasi-parallel bow shocks," Ann. Geophys. **22**, 2309–2313 (2004).
[65]K. A. Goodrich, R. Ergun, S. J. Schwartz, L. B. Wilson, D. Newman, F. D. Wilder, J. Holmes, A. Johlander, J. Burch, R. Torbert, Y. Khotyaintsev, P. Lindqvist, R. Strangeway, C. Russell, D. Gershman, B. Giles, and L. Andersson, "MMS observations of electrostatic waves in an oblique shock crossing," J. Geophys. Res. **123**, 9430–9442, https://doi.org/10.1029/2018JA025830 (2018).
[66]C. Lacombe, F. Pantellini, D. Hubert, C. C. Harvey, A. Mangeney, G. Belmont, and C. Russell, "Mirror and Alfvenic waves observed by ISEE 1–2 during crossings of the earth's bow shock," Ann. Geophys. **10**, 772–784 (1992).
[67]S. J. Schwartz, D. Burgess, and J. J. Moses, "Low-frequency waves in the Earth's magnetosheath: Present status," Ann. Geophys. **14**, 1134–1150 (1996).
[68]S. P. Gary, "The mirror and ion cyclotron anisotropy instabilities," J. Geophys. Res. **97**, 8519, https://doi.org/10.1029/92JA00299 (1992).
[69]R. E. Ergun, S. Tucker, J. Westfall, K. A. Goodrich, D. M. Malaspina, D. Summers, J. Wallace, M. Karlsson, J. Mack, N. Brennan, B. Pyke, P. Withnell, R. Torbert, J. Macri, D. Rau, I. Dors, J. Needell, P.-A. Lindqvist, G. Olsson, and C. M. Cully, "The axial double probe and fields signal processing for the MMS mission," Space Sci. Rev. **199**, 167–188 (2014).
[70]P.-A. Lindqvist, G. Olsson, R. B. Torbert, B. King, M. Granoff, D. Rau, G. Needell, S. Turco, I. Dors, P. Beckman, J. Macri, C. Frost, J. Salwen, A. Eriksson, L. Åhlén, Y. V. Khotyaintsev, J. Porter, K. Lappalainen, R. E. Ergun, W. Wermeer, and S. Tucker, "The spin-plane double probe electric field instrument for MMS," Space Sci. Rev. **199**, 137–165 (2014).
[71]R. B. Torbert, C. T. Russell, W. Magnes, R. E. Ergun, P.-A. Lindqvist, O. LeContel, H. Vaith, J. Macri, S. Myers, D. Rau, J. Needell, B. King, M. Granoff, M. Chutter, I. Dors, G. Olsson, Y. V. Khotyaintsev, A. Eriksson, C. A. Kletzing, S. Bounds, B. Anderson, W. Baumjohann, M. Steller, K. Bromund, G. Le, R. Nakamura, R. J. Strangeway, H. K. Leinweber, S. Tucker, J. Westfall, D. Fischer, F. Plaschke, J. Porter, and K. Lappalainen, "The FIELDS instrument suite on MMS: Scientific objectives, measurements, and data products," Space Sci. Rev. **199**, 105–135 (2014).
[72]R. P. Lepping, M. H. Acũna, L. F. Burlaga, W. M. Farrell, J. A. Slavin, K. H. Schatten, F. Mariani, N. F. Ness, F. M. Neubauer, Y. C. Whang, J. B. Byrnes, R. S. Kennon, P. V. Panetta, J. Scheifele, and E. M. Worley, "The WIND magnetic field investigation," Space Sci. Rev. **71**, 207–229 (1995).
[73]K. W. Ogilvie, D. J. Chornay, R. J. Fritzenreiter, F. Hunsaker, J. Keller, J. Lobell, G. Miller, J. D. Scudder, E. C. Sittler, R. B. Torbert, D. Bodet, G. Needell, A. J. Lazarus, J. T. Steinberg, J. H. Tappan, A. Mavretic, and E. Gergin, "SWE, a comprehensive plasma instrument for the WIND spacecraft," Space Sci. Rev. **71**, 55–77 (1995).
[74]C. Smith, J. L'Heureux, N. Ness, M. Acuña, L. Burlaga, and J. Scheifele, "The ACE magnetic fields experiment," Space Sci. Rev. **86**, 613–632 (1998).
[75]D. McComas, S. Bame, P. Barker, W. Feldman, J. Phillips, P. Riley, and J. Griffee, "Solar wind electron proton alpha monitor (SWEPAM) for the advanced composition explorer" Space Sci. Rev. **86**, 563–612 (1998).